Braz J Phys (2016) 46:254–261
DOI 10.1007/s13538-016-0408-5

SOCIEDADE BRASILEIRA DE FÍSICA

CONDENSED MATTER

AC Dielectric Properties and Positron Annihilation Study on Co and Ti Substitution Effect on Ca–Sr M-Hexaferrites

K. R. Mahmoud[1] · **M. R. Eraky**[1]

Received: 9 October 2015 / Published online: 1 March 2016

Abstract The dependence of AC conductivity σ_{AC}, dielectric constant $\acute{\varepsilon}$, and dielectric loss tangent tan δ on frequency and composition have been investigated at room temperature for polycrystalline $Ca_{0.5}Sr_{0.5}Co_xTi_xFe_{12-2x}O_{19}$ (where $0.0 \leq x \leq 0.8$) hexaferrites. It was found that the parameters σ_{AC}, ε', and tan δ have maximum values at $x = 0.4$ of the Co and Ti substitution. The behavior of σ_{AC}, ε', and tan δ with frequency and composition was explained on the basis of the hopping conduction mechanism and the Koops model. Positron annihilation lifetime spectroscopy (PALS) was used to investigate the defects and changes in electron density for hexaferrite samples. The PAL parameters (τ_1, I_1, τ_2, I_2, and mean lifetime) show that altering the doping percentage of the Co and Ti ions affects the size and concentration of defects. The results reveal that there are some large voids in the studied samples. The obtained results indicate the high sensitivity of the PALS technique to the enhanced structure changes with changing composition of the investigated samples and correlate the results with the measured electrical parameters.

Keywords AC conductivity · Dielectric · Polycrystalline · Hexaferrites · Positron annihilation lifetime spectroscopy

1 Introduction

The hexagonal ferrites (M type) have been attracting considerable attention in technological and scientific research because of their high electrical resistivity, high Curie temperature, high stability, and easy manufacturing. The M-type hexaferrites are very good dielectric materials, which can be used as a basic material for permanent magnets, magnetic recording media, microwave applications, and high-frequency devices [1–3]. It was reported that the grains formed during the sintering process of polycrystalline ferrites are electrically conductive, while the formed grain boundaries exhibit a dielectric behavior. At low frequencies, grain boundaries were found to be more effective while the ferrite grains are more effective at higher frequencies [4]. The grain boundaries formed during the sintering process may be due to superficial reduction or oxidation of crystallites as a result of direct contact with the firing atmosphere [4]. Thus, the ferrite can be considered as highly conductive grains separated by thin low conductive layers (grain boundaries) and behave as inhomogeneous dielectric materials. The AC electric field on the specimen is concentrated in the grain boundary regions. Therefore, the electric and dielectric properties are affected by the grain boundary phase and the defect distribution in ferrites.

Positron annihilation lifetime spectroscopy (PALS) is one of the powerful techniques for measuring the change in properties of structural defects in a wide variety of solids [5, 6]. In PALS, the Na-22 source decays by positron emission to a 1.27-MeV excited state of Ne-22. The 1.27-MeV gamma ray signals the positron birth and is used to start the lifetime clock. The clock is stopped by detection of the 511-keV annihilation gamma ray. When a positron emitted from the Na-22 source injected into solids, it thermalized and diffused to a depth of a few hundred micrometers. The positron either is directly annihilated with electrons in the sample, is trapped at certain sites in the material and lives longer, or may extract an electron from the surrounding material to form a positronium atom (Ps). Ps is formed in two states: a singlet state (*para*-Ps, *p*-Ps) and a triplet state (*ortho*-Ps, *o*-Ps). In both cases, the positron

✉ K. R. Mahmoud
kamalreyad@hotmail.com

[1] Physics Department, Faculty of Science, Kafrelsheikh University, El Gaish Street, Kafr El Sheikh 33516, Egypt

will eventually annihilate with an electron and will have a corresponding lifetime with a corresponding intensity for each state at the annihilation site. Each lifetime component has a corresponding intensity (I_1, I_2) relating to the number of annihilations occurring at a particular lifetime (τ_1, τ_2). Therefore, the detection of annihilation γ-rays due to trapping of positrons in annihilation sites is an indication of the lifetime of the impeded positrons in the ferrite sample which holds information about the electron density, concentration, and size of defects. The PAL technique was therefore employed successfully in studying several types of ferrites [7–11].

This paper presents an investigation of AC electrical conductivity and dielectric properties of CaSrCoTi M hexaferrites with changing composition and frequency at room temperature. The PALS technique is used in this work to investigate the structure of the prepared ferrite samples and correlate the results with that of the electrical properties.

2 Materials and Method

Co- and Ti-doped Ca–Sr M hexaferrite samples having the general formula $Ca_{0.5}Sr_{0.5}Co_xTi_xFe_{12-2x}O_{19}$ (where $x = 0.0$, 0.2, 0.4, 0.6, and 0.8) were prepared by a conventional double sintering ceramic method. Phase identification, crystal structure, lattice parameters, densities, and porosity of these samples were checked by X-ray powder diffraction measurements. The details of the method of preparation and X-ray measurements were reported earlier [12]. Figure 1 shows X-ray diffraction patterns of Ca–Sr M hexaferrite samples with Co and Ti contents. In spite of the presence of a weak peak belonging to the hematite phase for samples with $x = 0.2$–0.6 (plan 104), these samples still belong to the hexagonal phase with a percentage of more than 95 %. AC electrical resistivity and dielectric parameters were determined by the two-probe method using an LCR bridge (Model HIOKI 3532-50 LCR Hi tester) from 100 Hz to 5 MHz. The values of loss tangent tan δ and the capacitance (C) were determined directly by the bridge. The dielectric constant (ε') was calculated using the relation

$$\varepsilon' = Cd/\varepsilon_0 A \tag{1}$$

d is the thickness of the sample, A is the cross-sectional area of the sample, and ε_0 is the permittivity of free space ($\varepsilon_0 = 8.854 \times 10^{-12}$ F m^{-1}). The AC conductivity (σ_{AC}) of the samples was calculated by the relation

$$\sigma_{AC} = \omega \varepsilon' \varepsilon_0 \tan\delta \tag{2}$$

where ω is the angular frequency.

Positron lifetime measurements were carried out using a γ-ray spectrometer employing a fast-fast coincidence technique. It consists of two Bicron BC-418 plastic scintillation detectors and Ortec NIM modules, two 583 constant fraction differential discriminators (CFDD), DB643 delay ns box, 414A fast coincidence, and 566 time-to-amplitude converter (TAC) [13]. The data were acquired using an Ortec 919 multichannel analyzer (MCA). The time resolution of the spectrometer, measured with ^{60}Co source at ^{22}Na energy window setting, was ~350 ps (FWHM). A 15-μCi positron source was prepared using a droplet of ^{22}NaCl solution dried onto two identical Kapton foils (7.6 μm thick), which were afterward glued with epoxy glue. This source was sandwiched between two identical samples. The lifetime spectra were measured in air at room temperature. More than one million counts were accumulated for each spectrum, and each sample was measured at least three times. Deconvolutions were carried out through the computer code LT [14], with a suitable correction for the positrons annihilated in the Kapton. The lifetime spectra of the investigated samples were decomposed into two components. All these components were determined with the best-fitting parameter ranged from 1.0 to 1.2. The range of the experimental errors for the PAL parameters τ_1, τ_2, I_1, and I_2, determined over multiple measurements, was found to be <1.3 ps, <60 ps, 0.14 %, and 0.2 %, respectively. The mean lifetime of positrons τ_m, which reflects the overall performance of materials under the positron environment, is calculated by using the following formula:

$$\tau_m = (\tau_1 I_1 + \tau_2 I_2)/(I_1 + I_2) \tag{3}$$

3 Results and Discussion

3.1 Dielectric Behavior

The dielectric constant characterizes the most important electrical property of the dielectrics. The dielectric constant (or relative permittivity), ε^*, of a dielectric material placed in the AC electric field is a complex quantity because the orientation polarization lags behind the polarizing electric field as the frequency of the applied field is increased. The complex dielectric constant, ε^*, can be expressed as

$$\varepsilon^* = \varepsilon' + j\varepsilon'' \tag{4}$$

ε' is the real dielectric constant which characterizes the energy stored in the dielectric material, whereas the imaginary part ε represents the energy loss. The plots of the measured ε' and tan δ as a function of frequency are shown in Figs. 2 and 3 for the CaSrCoTi M ferrites, respectively. Both ε' and tan δ (at room temperature) decrease as frequency increases. It is noticed that there is much decrease in ε' and tan δ within the frequency range 0.1–10 kHz (2–4 on x-scale) and they are nearly unchanged above 100 kHz. This decrease in ε' and tan δ with increasing frequency indicates the formation of

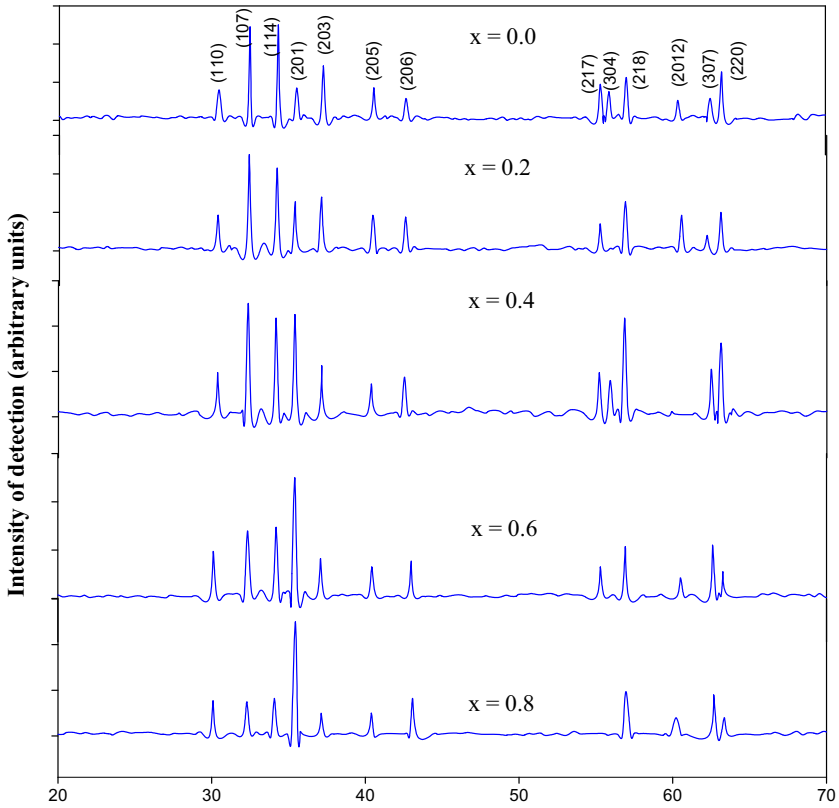

Fig. 1 XRD patterns of $Ca_{0.5}Sr_{0.5}Co_xTi_xFe_{12-2x}O_{19}$ hexaferrites at different concentrations of Co–Ti ions

heterogeneous structures with the ferrite under investigation, and this is a normal dielectric behavior in ferrites [15]. Moreover, from Fig. 3, we notice that tan δ has maxima for the samples with $x=0$ and 0.8 at 200 and 190 Hz, respectively, while it showed maxima at 316, 437, and 240 Hz for samples with $x=0.2$, 0.4, and 0.6, respectively. The appearance of relaxation peaks for tan δ was observed in many substituted ferrites [16, 17]. The decrease in ε' and tan δ with increasing frequency takes place when the hopping frequency of the charge carrier (electron and hole) cannot follow the alternating frequency of the applied AC electric field beyond a certain critical frequency [18]. All samples have high values of log ε' ranged from 3 to 6.5 at 100 Hz. These high values of ε' were observed for SrPb M hexaferrites [19], BaCoZn-W hexaferrites [20], Mg–Zn [4], Cu–Ge [21], and Li–Ni [22] ferrites. The high values of ε' and tan δ at low frequencies are due to predominance of species like Fe^{2+} ions, interfacial dislocation pileup, oxygen vacancies, grain boundary defects, etc. [23, 24]. The decreasing of both ε' and tan δ with increasing frequency could be explained on the basis of the Maxwell–Wagner theory [23, 24] and Koops theory [15]. The dielectric material is assumed to be composed of well-conducting grains, which are separated by thin layers of poorly conducting grain boundaries [15]. The grain boundaries are found to be more effective at lower frequencies, while grains are effective at higher frequencies [15, 25]. The dielectric relaxation is expected as any of the predominant species contribute to the different mechanisms of polarization lag behind the applied field, i.e., they cannot follow the changes in the applied field over a certain frequency limit, as the frequency increases.

Iwauchi reported that there is a strong correlation between the conduction mechanism and the dielectric behavior of ferrites [26]. Hudson has shown that the materials with low resistivity exhibit high dielectric loss and vice versa [27].

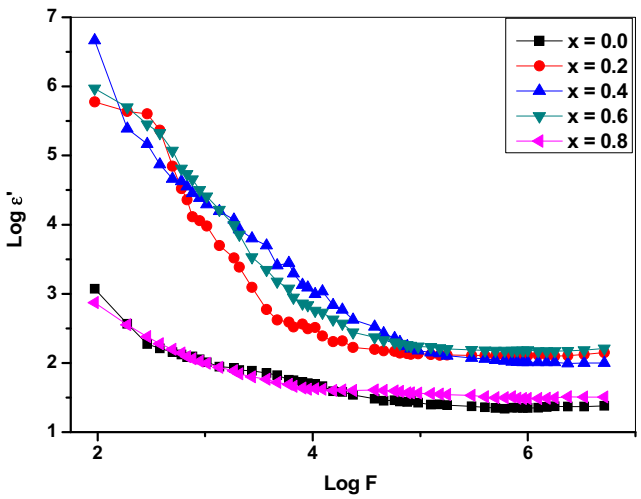

Fig. 2 Variation of real dielectric constant log ε' with frequency at room temperature for $Ca_{0.5}Sr_{0.5}Co_xTi_xFe_{12-2x}O_{19}$ hexaferrites at different concentrations of Co–Ti ions

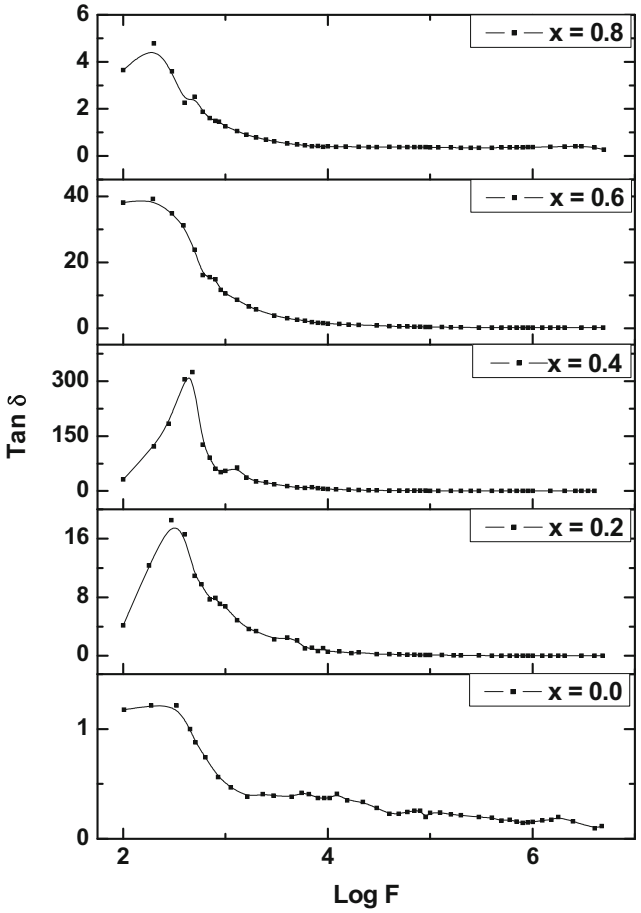

Fig. 3 Variation of dielectric loss factor tanδ with frequency at room temperature for $Ca_{0.5}Sr_{0.5}Co_xTi_xFe_{12-2x}O_{19}$ hexaferrites at different concentrations of Co–Ti ions. The *solid lines* are guides to the eye

According to Iwauchi [26] and Hudson [27], our results for ε' reflect a good correspondence between ε' and resistivity, where the highly resistive samples with $x=0$ and 0.8 [12] have a low dielectric constant. The loss tangent relaxation peaks can be observed when the hopping frequency of charge carriers coincides with the frequency of the external electric field. However, the samples with $x=0.0$ and 0.8 showed a maximum peak at low frequencies. For the other samples with $x=0.2$ and 0.6, the relaxation loss peaks are predicted at moderate frequencies. The sample with $x=0.4$ may have a loss peak at a higher frequency. The relaxation peak in loss tangent tan δ at room temperature may be related to the amount of Fe^{2+}/Fe^{3+} and Co^{3+}/Co^{2+} ions in octahedral B-sites. The condition of observing maxima in the dielectric loss factor tan δ of a dielectric material is given by the relation $\omega\tau=1$, where $\omega=2\pi f_{max}$ and τ is the relaxation time. The relaxation time τ is related to the jump probability per unit time (p) by the relation $\tau=1/(2p)$, consequently the loss frequency proportional to the jumping probability ($f_{max}\alpha p$). Therefore, maxima can be observed when the jump or hopping frequency of charge carriers between Fe^{2+}/Fe^{3+} or Co^{3+}/Co^{2+} ions becomes approximately equal to the frequency of the applied field [25, 28]. Thus, the position of the loss peak depends on the number of Fe^{2+}/Fe^{3+} and Co^{3+}/Co^{2+} ions in the octahedral B-site or hopping probability p. It was found that the samples with $x=0$ and 0.8 showed a higher DC resistivity at room temperature [12] due to low concentration of Fe^{2+}/Fe^{3+} and Co^{3+}/Co^{2+} ions and/or low value of p, consequently low relaxation frequency f_{max} ($f_{max}=200$ and 190 Hz, respectively). The sample with $x=0.4$ has a high value of f_{max} ($f_{max}=437$ Hz) because it has a low DC resistivity at room temperature or sufficient amount of Fe^{2+}/Fe^{3+} and Co^{3+}/Co^{2+} on B-sites [12].

3.2 Composition Dependence

The effects of replacing Fe^{3+} ions with Co^{2+} and Ti^{4+} ions on real AC electrical conductivity σ_{AC}, real dielectric constant ε', and dielectric loss factor tan δ are illustrated in Figs. 4, 5, and 6, respectively. $\sigma_{AC}(x)$, $\varepsilon'(x)$, and tan $\delta(x)$ were plotted at selected frequencies of 0.1, 1, 10, and 100 kHz and 1 MHz. Each of σ_{AC}, ε', and tan δ increase with increasing replacement of Fe^{3+} ions by Co^{2+} and Ti^{4+} ions to become maxima for $x=0.4$ and started to decrease for $x>0.4$. It is noticed that for a certain concentration (x), the conductivity increases with increasing frequency (Fig. 4) while ε' and tan δ showed decreasing values (Figs. 5 and 6). This behavior of σ_{AC}, ε', and tan δ gives a qualitative agreement with results obtained by Abo Elata et al. [29] for substituted Ba hexaferrite particularly for $x>0.4$. It was reported that the predominant conduction mechanism in substituted Ca–Sr M hexaferrite is due to the hopping process of electrons between Fe^{2+}/Fe^{3+} and holes between Co^{3+}/Co^{2+} ions. Fe^{2+} and Co^{3+} ions may be presented during the sintering process [12]. The M hexaferrites contain five positions for the Fe^{3+} ions, three octahedral B-sites (12k, 2a, and $4f_2$ sites), one

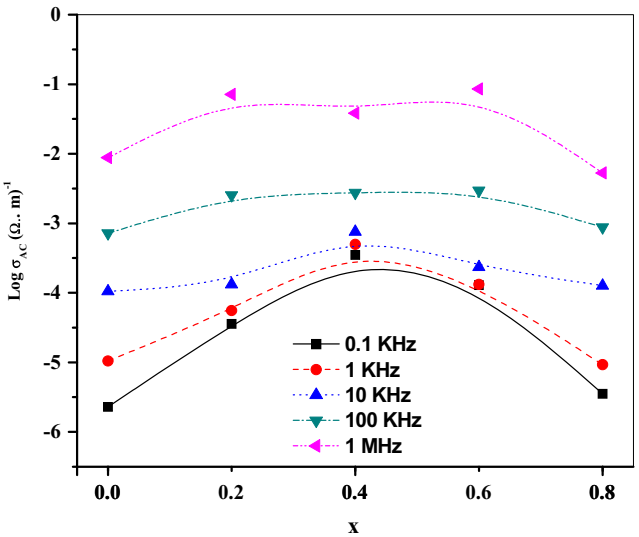

Fig. 4 Variations of AC conductivity (log σ_{AC}) with Co and Ti contents (x) for $Ca_{0.5}Sr_{0.5}Co_xTi_xFe_{12-2x}O_{19}$ hexaferrites at room temperature

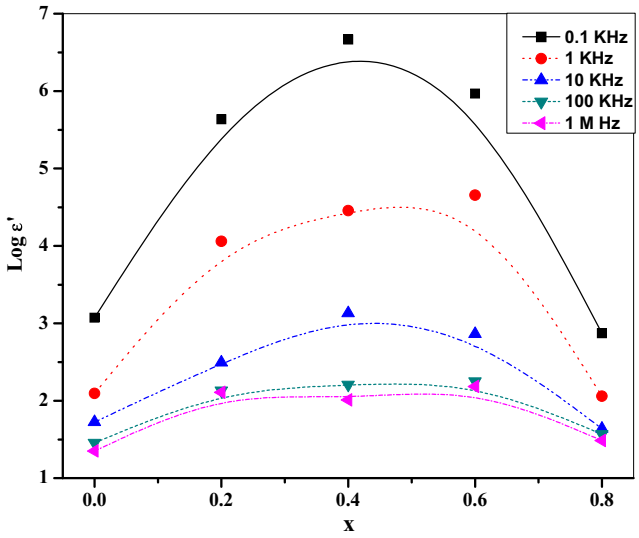

Fig. 5 Variations of dielectric constant (log ε') with Co and Ti contents (x) for $Ca_{0.5}Sr_{0.5}Co_xTi_xFe_{12-2x}O_{19}$ hexaferrites at room temperature

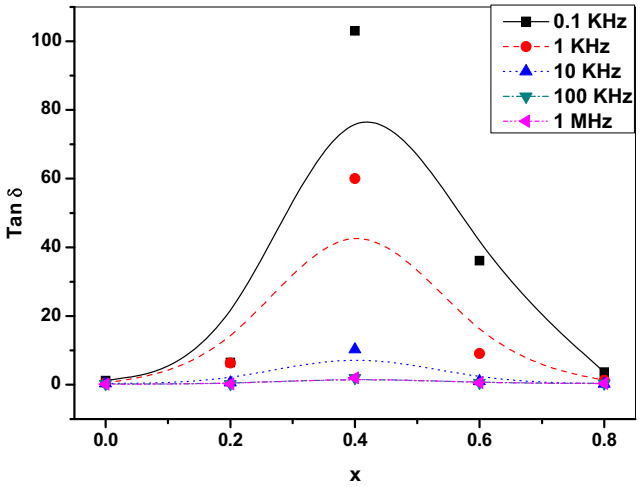

Fig. 6 Variations of dielectric loss tangent (tanδ) with Co and Ti contents (x) for $Ca_{0.5}Sr_{0.5}Co_xTi_xFe_{12-2x}O_{19}$ hexaferrites at room temperature

tetrahedral A-site ($4f_1$ site), and one named C-site bi-pyramid (2b site) which is surrounded by five oxygen ions. The charge carrier hopping between A and B-sites has a very small probability compared with that for B–B hopping. Hopping between A–A sites does not occur because any formed ferrous ion Fe^{2+} prefers to occupy the B-site only [19]. Thus, as the replacement of Fe ions by Co and Ti ions increases, the concentration of Fe^{2+} and Co^{3+} in B-sites increases (to keep electric neutrality in the site) and the hopping process increases gradually; therefore, the values of σ_{AC}, ε', and tan δ increased up to $x=0.4$ (Figs. 3, 4, and 5). The decreasing in σ_{AC}, ε', and tan δ for samples with $x>0.4$ may be due to the increasing in porosity up to $x=0.8$ because the porous obstructs the flow of carriers [30], and/or due to the increasing in hopping distance. Using X-ray data, the lattice parameters and cell volume of the samples were calculated. It is shown that a-parameter increases up to $x=0.4$ after which it becomes nearly constant, while c-parameter increases gradually up to $x=0.8$ [12]. This means that at $x>0.4$, the hopping distance may become large enough to obstruct the electron and hole hopping and consequently contribute in the decreasing of σ_{AC}, ε', and tan δ. Also, the average crystallite size D was calculated using XRD data [12] and the Deby–Sherrer formula [31] for all the studied samples (Table 1). We notice a decrease in crystallite size values with increasing Co and Ti contents up to $x=0.4$, after which the crystallite size slightly increases.

The charge carrier concentration (n) for CaSrCoTi M hexaferrites was determined at room temperature from the relation [32]

$$n = N_A D_m P_{Fe}/M_w \quad (5)$$

N_A is Avogadro's number, D_m is the bulk density, P_{Fe} is the number of iron ions in the chemical formula $Ca_{0.5}Sr_{0.5}Co_xTi_xFe_{12-2x}O_{19}$, and M_w is the molecular weight. The calculated values for the charge carrier concentration (n) are shown in Table 1. From Table 1, we notice a little increase in the charge carrier concentration with increasing Co and Ti up to $x=0.4$, after which it showed a rapid decrease at $x>0.4$. The presence of Ti^{4+} at the octahedral B-site acts as a trap for electrons by forming electrostatic bonds with Fe^{2+} ions. At pure and low substituted samples, the effect of Ti^{4+} ions is negligible; therefore, the concentration of the charge carrier increased for $x<0.4$. However, at higher substitution, the amount of Ti^{4+} became sufficient to reduce the carrier concentration.

3.3 Positron Annihilation Studies

The two lifetime components τ_1 and τ_2 with intensities I_1 and I_2 were determined from the PAL spectra of the investigated samples as shown in Figs. 7 and 8. Figure 7 shows the variation of the lifetime component τ_1 and its intensity I_1 as a function of Co and Ti contents x. The results showed that the measured range of τ_1 lifetime component was 194–210 ps with the relative intensity ranging from 98.7 to 99.1 % for all studied samples. In this case, the shortest lifetime (τ_1) represents the weighted average of positron lifetimes at the grain boundary defects as well as the lifetime corresponding to annihilation with free electrons residing in the grain boundaries. The relative intensity I_1 is the fraction of positron annihilated at the grain boundary defects. It is clear from the data in Fig. 7 that there was a rapid increase of the positron lifetime (τ_1) with increasing Co and Ti contents up to $x=0.4$. This can be explained if we consider the effect of change in the calculated values of crystallite size D for the investigated samples (Table 1), which showed a decrease with increasing composition parameters up to $x=0.4$. It is reported that when the grain size of the sample is decreased, the

Table 1 Values of crystallite size (D), cell volume (v), porosity (P), and charge carrier concentration (n) calculations for the system SrCa–CoTi M hexaferrites (given in ref. [12])

	Co–Ti content, x				
	0.0	0.2	0.4	0.6	0.8
Crystallite size, D (nm)	466	347	275	342	385
Cell volume, v (Å)^3	684.64	688.21	692.49	690.98	692.35
Porosity, P (%)	13.76	7.13	6.97	9.09	14.96
$n \times 10^{+23}$ cm^{-3}	3.02324	3.13089	3.00934	2.84174	2.55495

thickness of grain boundaries is increased and the number of defects due to grain boundaries is increased [33]. Consequently, the electron density inside the grain boundaries decreased which leads to an increase in the values of τ_1 and a decrease of I_1 up to $x=0.4$ as shown in Fig. 7. An opposite behavior was shown for I_1 in Fig. 7 for $x>0.4$. The I_1 increased due to the increase of crystallite size D which leads to a decrease in the thickness of the grain boundaries, and consequently, the electron density increased in these samples. The values of τ_1 must be decreased for the samples with $x>0.4$ according to the last interpretation. But the data in Fig. 7 confirms unlike this which showed a slight increase of τ_1 with $x>0.4$. This can be attributed to the rapid decrease of charge carrier concentration (n) (see Table 1) which leads to reduced electron density in the grain boundary causing a slight increase of τ_1 with $x>0.4$. It can be concluded that the PAL technique measures the changes in defects and free volume which in turn can be one of the reasons for changing electrical properties of the investigated samples.

Figure 8 shows the variations in the lifetime component τ_2 and its intensity I_2 with Co and Ti contents x. The range of τ_2 is 1174–1259.3 ps with relative intensity $I_2=0.89$–1.23 % for the studied samples. τ_2 is corresponding to a small fraction of *ortho*-positronium (*o*-Ps) atoms as the longest lifetime component (>900 ps) is assigned to the pick-off annihilation of *o*-Ps atoms formed inside large voids for bulk [7] and/or arises from the positrons trapped in the nanovoids available at the intersection of the grain boundaries [34]. Although the contributions of I_2 are <1.3 %, their existence reveals that there are some voids with irregular distribution in the studied samples. The curves of τ_2 and I_2 in Fig. 8 tend to form peak points at $x=0.4$, decreasing at both sides. The qualitative behavior of τ_2 (Fig. 8) and the calculated values for cell volume (Table 1) are more consistent. It is reported that the large particle size reduces the concentration of nanovoids present at the intersection of grain boundaries [34]. Accordingly, the increase of I_2 up to $x=0.4$ can be attributed to the decrease of the crystallite size, which

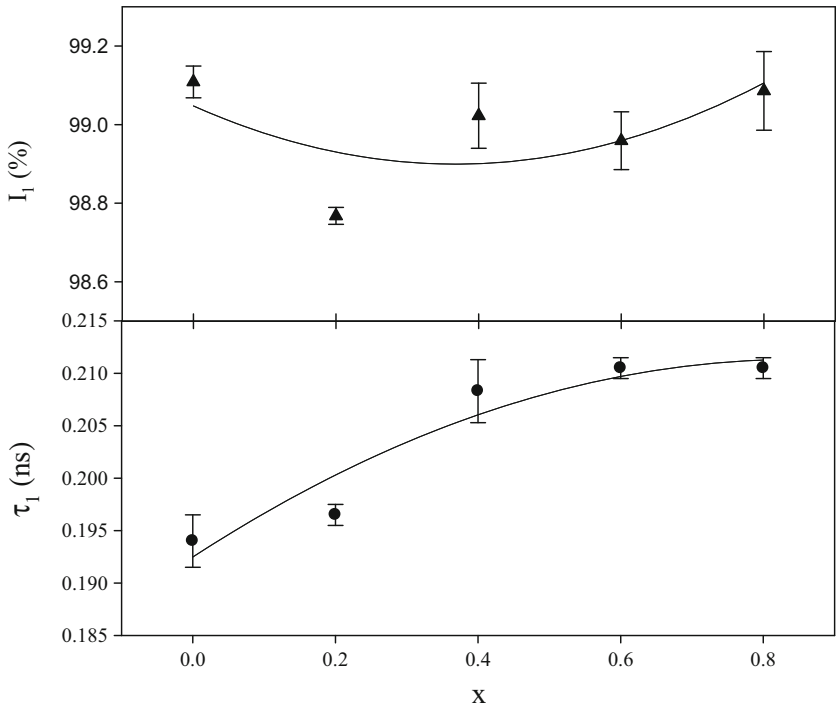

Fig. 7 The dependence of the lifetime component τ_1 and its corresponding intensity I_1 on Co and Ti contents, x, for the system $Sr_{0.5}Ca_{0.5}Co_xTi_xFe_{12-2x}O_{19}$ hexaferrites at room temperature

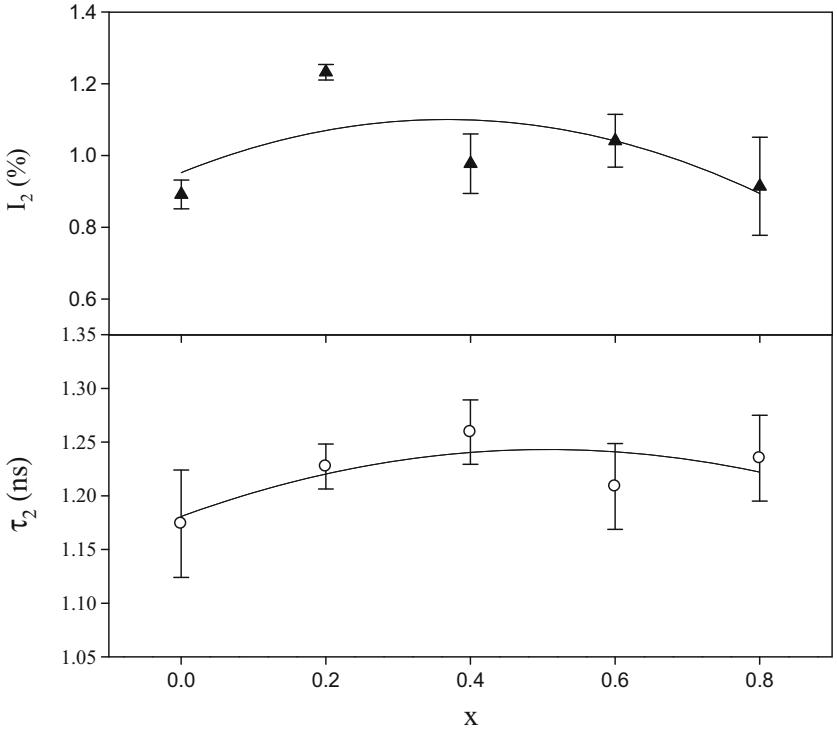

Fig. 8 The dependence of the lifetime component τ_2 and its corresponding intensity I_2 on Co and Ti contents, x, for $Sr_{0.5}Ca_{0.5}Co_xTi_xFe_{12-2x}O_{19}$ hexaferrites at room temperature

increases the concentration of voids present at the intersection of grain boundaries. An opposite behavior was shown for I_2 at $x>0.4$ which decreased as the crystallite size increased.

The variation of the mean lifetime τ_m, which reflects the average changes in the sample structure (electron density, defect size, etc.), as a function of Co and Ti contents is shown in Fig. 9. For a given type (size) of defect, the higher the defect density, the larger will be the value of τ_m [35]. The values of τ_m were seen to increase with increasing Co and Ti contents, and the curve in Fig. 9 shows an inflection wide hump at $x=0.6$. Consequently, the increase in τ_m can be attributed to the presence of a high density of positron trapping centers.

4 Conclusion

The variation of AC conductivity σ_{AC}, dielectric constant ε', and dielectric loss tangent tan δ on frequency and composition has been investigated at room temperature for polycrystalline $Ca_{0.5}Sr_{0.5}Co_xTi_xFe_{12-2x}O_{19}$ (where $0.0\leq x\leq 0.8$) hexaferrites. ε' has a normal trend with increasing frequency, whereas tan δ showed relaxation loss peaks at certain frequencies. The behavior of σ_{AC}, ε', and tan δ with frequency and composition was explained on the basis of the hopping conduction mechanism and the Koops model. Positron lifetime results showed a significant dependence on Co and Ti contents. The PAL parameters (τ_1, I_1, τ_2, I_2, and τ_m) are reflecting that the electron

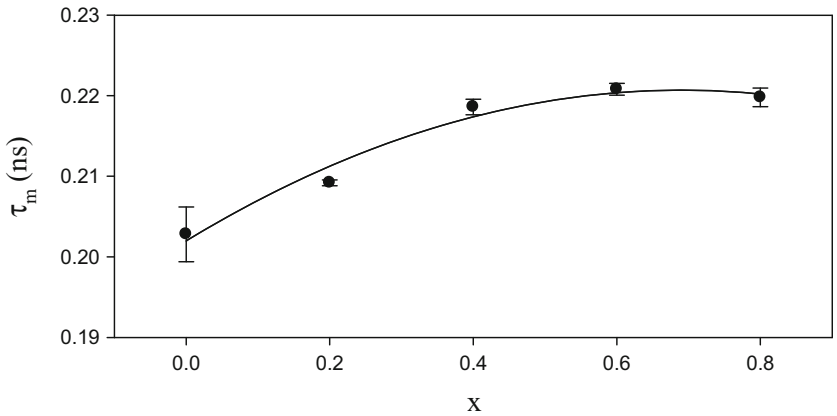

Fig. 9 The variation of the mean lifetime, τ_m (ns), with Co and Ti contents (x) for $Sr_{0.5}Ca_{0.5}Co_xTi_xFe_{12-2x}O_{19}$ hexaferrites at room temperature

density and the size and concentration of the defects are affected by the replacement of Fe^{3+} by Co and Ti ions. Therefore, the PAL results indicated the sensitivity of the positron lifetime to study the changes in density and size of defects, which in turn can be one of the reasons for changing electrical properties of substituted M hexaferrites.

References

1. V.B. Kawade, G.K. Bichile, K.M. Jadhav, Mater. Lett. **42**, 33 (2000)
2. G. Albanese, A. Deriu, E. Lucchii, G. Slokar, J. Appl. Phys. A **26**, 45 (1981)
3. C.S. Kim, S.W. Lee, S. Yong An, J. Appl. Phys. **87**, 6244 (2000)
4. M.A. El Hiti, J. Magn. Magn. Mater. **192**, 305 (1999)
5. Y.C. Jean, P.E. Mallon, D.M. Schrader, *Principles and Applications of Positron & Positronium Chemistry* (World Scientific Publishing Co. Pte. Ltd., New Jersey, 2003)
6. A. Dupasquier Jr., A.P. Mills, *Positron Spectroscopy of Solids* (Ios Press, Amsterdam and SIF, Bologna, 1995)
7. H.E. Hassan, T. Sharshar, M.M. Hessien, O.M. Hemeda, Nucl. Instrum. Meth. B **304**, 72 (2013)
8. S. Ghosh, P.M.G. Nambissan, R. Bhattachary, Phys. B **353**, 75 (2004)
9. A.M. Samy, N. Mostafa, E. Gomaa, The Open Ceram. Sci. J. **1**, 1 (2010)
10. P.M.G. Nambissan, C. Upadhyay, H.C. Verma, J. Appl. Phys. **93**, 6320 (2003)
11. H. Klym, A. Ingram, O. Shpotyuk, J. Filipecki, Visnyk Lviv Univ. Ser. Physic. **40**, 200 (2007)
12. M.R. Eraky, J. Magn. Magn. Mater. **324**, 1034 (2012)
13. K.R. Mahmoud, S. Al-Sigeny, T. Sharshar, H. El-Hamshary, Radiat. Phys. Chem. **75**, 590 (2006)
14. J. Kansy, Nucl. Instrum. Meth. A **374**, 235 (1996)
15. C.G. Koop's, Phys. Rev. **83**, 121 (1951)
16. M.K. Fayek, S.S. Ata-Allah, H.A. Zayed, M. Kaiser, S.M. Ismail, J. Alloys Compd. **469**, 9 (2009)
17. A.V. Ramana Reddy, G. Ranga Mohan, D. Ravinder, B.S. Boyanov, J. Mater. Sci. **34**, 3169 (1999)
18. A.D. Sheikh, V.L. Mathe, J. Mater. Sci. **43**, 2018 (2008)
19. S. Hussain, A. Maqsood, J. Alloy. Compd. **466**, 293 (2008)
20. M.A. Ahmed, N. Okasha, R.M. Kershi, J. Magn. Magn. Mater. **321**(24), 3967 (2009)
21. S.A. Mazen, A.M. El Taher, Solid State Commun. **150**, 1719 (2010)
22. M.F. Al-Hilli, S. Li, K.S. Kassim, J. Magn. Magn. Mater. **324**, 873 (2012)
23. J.C. Maxwell, *Electricity and Magnetism*, vol. 2 (Oxford University Press, New York, 1973)
24. K.W. Wagner, E.L. Heilman, Ann. Phys. **40**, 818 (1993)
25. M.A. Ahmed, M.A. El Hiti, M.A. Amer, M.K. El Nimr, J. Mater. Sci. Lett. **16**, 1076 (1997)
26. K. Iwauchi, Jpn. J. Appl. Phys. **10**, 1520 (1971)
27. A.S. Hudson, Marconi Rev. **37**, 43 (1968)
28. L.I. Rabinkin Z.I. Novikova. Izv.Acd. Nauk, USSR, Minsk. p146 (1960).
29. A.M. Abo El Ata, M.A. El Hiti, M.K. El Nimr, J. Mater. Sci. Lett. **17**, 409 (1998)
30. R.S. Devan, Y.D. Kolekar, B.K. Chougule, J. Phys.-Condens. Mat **18**, 9809 (2006)
31. B.D. Cullity. Addison Wesley, MA. 1978.
32. S. Hussain, A. Maqsood, J. Magn. Magn. Mater. **316**, 73 (2007)
33. A.M. Samy, N. Mostafa, E. Gomaa, Appl. Surf. Sci. **252**, 3323 (2006)
34. S.K. Sharma, P.K. Pujari, K. Sudarshan, D. Dutta, M. Mahapatra, S.V. Godbole, O.D. Jayakumar, A.K. Tyagi, Solid State Commun. **149**, 550 (2009)
35. A. Banerjee, S. Bid, H. Dutta, S. Chaudhuri, D. Das, S.K. Pradhan, J. Asian Ceram. Soc. **1**, 356 (2013)